Shap. Mem. Superelasticity
https://doi.org/10.1007/s40830-025-00532-1

ORIGINAL RESEARCH ARTICLE

Design of (TiHfZr)(NiCoCu) High-Entropy Shape Memory Alloys: From Firstov's Experiments to Data-Driven Approach

L. Peltier[1] · L. Thiercelin[1] · F. Meraghni[1]

Received: 19 September 2024 / Revised: 17 December 2024 / Accepted: 14 February 2025

Abstract This paper deals with the design of (TiHfZr)(NiCoCu) high-entropy and high-temperature shape memory alloys (HE-HT-SMAs). It explains the chronology and the progress of this design starting from the experimental work of Georgi Firstov initiated in the 2015s until the advent of data-driven alloy approaches. A state-of-the-art (TiHfZr)(NiCoCu) HE-HT-SMA family is presented and enriched by a database used as input for a data-driven approach. The paper then focuses on the comparison of martensitic transformation temperatures provided by: (i) the experimental work of Firstov et al. started in 2015, (ii) other recent experimental studies and, (iii) those predicted by two numerical approaches. The first approach consists of a linear regression model proposed by Peltier et al., while the second one is proposed and enriched by Thiercelin et al. using a data-driven technique (random forest regression). The results from the data-driven approach yield accurate predictions that align with the experimental data from both the literature and previous studies. Thus demonstrating the importance of physics-informed, inspired techniques to optimize the design of future alloys, in particular HE-HT-SMAs.

Keywords High-entropy alloys · High-temperature shape memory alloys · Martensitic transformation · Shape memory effect · Physics-informed machine learning · Design of "NiTi-like" alloys

✉ F. Meraghni
fodil.meraghni@ensam.eu

[1] Arts Et Métiers Institute of Technology, CNRS, LEM3-UMR 7239, 57000 Metz, France

Introduction

Quasi-equiatomic NiTi binary alloy discovered inadvertently by William Buehler in 1963 [1, 2] has become the most widely studied and used shape memory alloy (SMA) for actuation applications. Depending on the Ni content, the NiTi binary alloy can be either austenitic or martensitic at room temperature with a martensitic start temperature (M_s) ranging from − 100 °C for 51.1 at.% Ni to 70 °C for 49.5 at.% Ni [3, 4]. The NiTi binary system has been improved by adding alloying elements whose physical properties are quite close to Ni, such as Cu, Co, Fe, Pd, Pt, Au and close to Ti, such as Zr or Hf [5]. NiTi-like are alloys containing alloying elements in addition to Ni and Ti, but which retain the martensitic phase transformation. Based on the metallurgy of ternary and quaternary systems, the transformation temperatures are currently highly improved and led to the design of high-temperature SMAs (HT-SMAs) whose M_s temperature is up to 300 °C [5]. However, these ternary or quaternary high-temperature shape memory alloys (HT-SMAs) have drawbacks, such as short service life [6–8] and require rare and expensive alloying elements. To overcome these limitations, some research works have been carried out using the strategy of high-entropy alloys (HEA). These alloys are generally containing at least five elements in equiatomic concentration. They are characterized by high mechanical strength due to the distortion of the crystallographic lattice, high thermal stability due to sluggish diffusion and the synergy of several properties of the alloying elements thanks to the cocktail effect. The first attempt to develop the concept of Complex Concentrated Alloys (CCAs) has been initiated by Achard in 1788 [9], who proposed more than 900 different combinations of alloys, including equiatomic alloys composed of 5 to 7 alloying elements. Several years after,

Published online: 11 March 2025

in 2004, Brian Cantor [10, 11] promoted the HEA concept as a particular case of equiatomic CCAs.

In 2015, Firstov et al. proposed an innovative study devoted to high-temperature NiTi-like alloys containing at least 5 elements, with the following compositions: $(TiHfZr)_{50}(NiCu)_{50}$ and $(TiHfZr)_{50}(NiCoCu)_{50}$ [12]. These alloys are called High-Temperature and High-Entropy Shape Memory Alloys (HE-HT-SMAs). Firstov has demonstrated that HT-SMAs can be produced using the high-entropy strategy, without expensive or strategic elements, such as gold, platinum or palladium [13–20]. In Firstov et al. [12, 21–23], the chemical composition of binary NiTi alloys has been modified by partially replacing the titanium content with the elements Zr and Hf, while Ni has been partially replaced by Cu and Co. This equivalent element substitution strategy has been explored and successfully implemented in recent studies by Peltier et al. [24–26]. The authors have demonstrated that these new alloys exhibit similar reversible austenite/martensite transformation features compared to binary NiTi alloys. At high temperatures, the developed HEAs exhibit stabilized superelastic and shape memory effects compared to NiTi [24]. Indeed, the high-entropy strategy has been demonstrated as a promising way to improve the high-temperature thermal fatigue response of SMAs. It is worth noticing that the alloys proposed by Firstov have been studied in their as-cast metallurgical state. The as-cast state refers to the metallurgical condition in which multiple phases are present, including dendritic phases, precipitates, and intermetallic compounds, all of which contribute to delaying the martensitic transformation. Indeed, the heterogeneity of the metallurgical state brings about a progressive martensitic transformation increasing hence the gap between the transformation temperature M_s and M_f. For instance, the alloy $(TiHfZr)_{50}Ni_{25}Cu_{15}Co_{10}$ proposed by Firstov [12] has been characterized by a temperature M_s up to 157 °C. The same alloy has been studied later by Chen [27], Yaacoub [28] and Rehman in a homogenized metallurgical state. The homogenized state is a metallurgical state obtained after heat treatments above 800 °C to achieve a predominant single-phase state (austenite or martensite) by removing the residual phases observed in the as-cast state (Peltier et al. [24], Piorunek et al. [29]).

The measured M_s temperatures provided by these authors have been comparable but less than the ones given by Firstov for the same alloy but in an as-cast metallurgical state. For this reason, it is strongly recommended that all developed HE-SMAs must be studied in a homogenized metallurgical state using appropriate heat treatments. In fact, this will result in a narrow DSC thermogram peak corresponding to the martensite transformation, providing hence a consistent M_s temperature representative of the alloy being developed.

Artificial intelligence-based approaches are currently being developed for the design of HE-SMAs and the prediction of their transformation temperatures, and they are particularly suitable for HT-SMAs, as presented in the relevant review by Hart et al. [30]. It should be noted that some of these physics-informed machine learning tools are easy-to-use open-source online databases and models, such as Thiercelin et al. [31] or Liu et al. [32], while others are more difficult to use due to the lack of database access or scripting [33–36].

In the present paper, the design process (TiHfZr)(NiCoCu) HE-HT-SMAs family has been revisited using a data-driven approach enriched by two databases. The first one includes all the NiTi-like alloys combining the elements Ni, Cu, Co, Ti, Zr, and Hf regardless of their metallurgical state. This database (noted hereafter "global database") contains binary, ternary, quaternary, quinary, and senary (TiHfZr)(NiCoCu) HE-HT-SMAs. The second database noted hereafter "reduced database" consists of a part of the global one considering only the NiTi-like alloys having been submitted to homogenization heat treatment, where the difference between M_s and M_f is less than 50 °C [31]. To this end, two prediction models have been deployed for estimating the martensitic transformation temperature. The first model is founded on linear regression proposed by Peltier et al. [37]. It has been applied exclusively on homogenized HE-HT-SMAs. The second prediction model utilizes a physics-informed machine learning approach. It has been deployed on the "global database" and then on the reduced one.

The paper aims to enhance the design process of the (TiHfZr)(NiCoCu) HE-HT-SMAs family, starting from Firstov's 2015 experiments, by incorporating data-driven algorithms and techniques to accelerate HE-SMA design. It traces the evolution of the (TiHfZr)(NiCoCu) design strategy over time, from one based entirely on empirical methods to a more advanced approach that integrates predictive models. The complexity of these models has progressively increased, evolving from linear regression to physics-informed machine learning algorithms.

The present paper is structured as follows: the second section is devoted to the works performed by Firstov et al. [12, 21–23] that initiated the HE-HT-SMAs development and design. The third section is devoted to experimental studies inspired by the original works by Firstov emphasizing the relevance of the metallurgical state on the martensitic transformation in HE-HT-SMAs. The fourth part presents the gathered databases of NiTi-like alloys that allow the jump to a data-driven approach toward reliable representation of a pseudo-ternary covering all the alloying composition space. The comparison of the predicted M_s values, presented in Sections. "Comparison of the Numerical Predictions Against Rehman et al. Experimental Results" and "Comparison of the Numerical Predictions Considering Other Compositions," highlights the impact of the metallurgical state on the variability of M_s values found in the open literature and

those measured by the authors in previous studies. Some concluding remarks and prospects are drawn in the last part of the paper.

Analysis of the Studies on HE-HT-SMAs Carried Out by Firstov

To study the compositional space of HE-SMAs (TiHfZr)(NiCoCu), Firstov started by setting the proportion of each Ti-like element (Ti, Hf, and Zr) to 16.67 at.%. The compositional space of HE-SMAs (TiHfZr)(NiCoCu) is thus reduced to 3 dimensions, i.e., the proportion of each Ni-like element (Ni, Cu, and Co) can vary from 0 to 25 at.% each. The system is shown in Fig. 1a as a pseudo-ternary diagram $(TiHfZr)_{50}(Ni_XCo_YCu_Z)_{50}$. Firstov et al. [12, 21–23] proposed and analyzed 8 NiTi-like alloys, whose chemical compositions are given in Table 1. For this purpose, X-ray diffraction (XRD) has been employed to identify the phases present at room temperature, for the developed 8 alloys. The results highlight a zone dominated by the martensite B19' phase, which is observed in alloys 1, 2, 3, 4, and 5, whose diffractograms are shown separately in Fig. 1b. In addition, those diffractograms highlight the presence of martensite peaks B19' and austenite peaks B2.

In the pseudo-ternary diagram, the widest zone is that of the austenitic B2 phase, which includes alloys 6, 7, and 8. The corresponding diffractograms of alloys 6, 7, and 8 are shown in Fig. 1c. It should be noted that Firstov did not provide the transformation temperatures of the 8 alloys shown

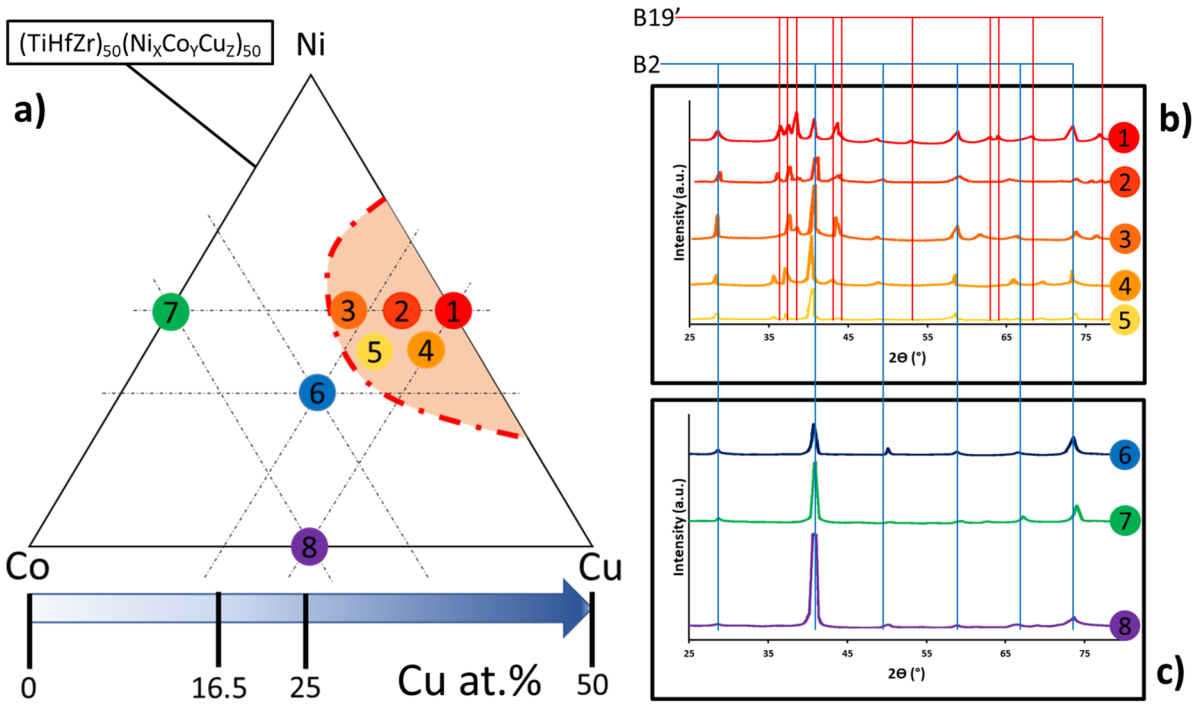

Fig. 1 Pseudo-ternary diagram for $(TiHfZr)_{50}(Ni_XCo_YCu_Z)_{50}$ alloys: **a** positioning of the compositions studied by Firstov on the $Ni_XCo_YCu_Z$ ternary diagram proposed at the ESOMAT 2018 international conference in Metz, **b** diffractograms of alloys with martensitic and austenitic phases, **c** diffractograms of austenitic alloys

Table 1 Composition of HE-SMAs studied by Firstov [12, 21–23]

Alloys		Alloying composition (at.%)					
		Ti	Hf	Zr	Ni	Co	Cu
1	$(TiHfZr)_{50}Ni_{25}Cu_{25}$	16.667	16.667	16.667	25	0	25
2	$(TiHfZr)_{50}Ni_{25}Co_5Cu_{20}$	16.667	16.667	16.667	25	5	20
3	$(TiHfZr)_{50}Ni_{25}Co_{10}Cu_{15}$	16.667	16.667	16.667	25	10	15
4	$(TiHfZr)_{50}Ni_{20}Co_5Cu_{25}$	16.667	16.667	16.667	20	5	25
5	$(TiHfZr)_{50}Ni_{20}Co_{10}Cu_{20}$	16.667	16.667	16.667	20	10	20
6	$(TiHfZr)_{50}Ni_{16.667}Co_{16.667}Cu_{16.667}$	16.667	16.667	16.667	16.667	16.667	16.667
7	$(TiHfZr)_{50}Ni_{25}Co_{25}$	16.667	16.667	16.667	25	25	0
8	$(TiHfZr)_{50}Co_{25}Cu_{25}$	16.667	16.667	16.667	0	25	25

in Fig. 1. Only the X-ray diffraction technique is used to determine the present phases and to discriminate martensite B19' from austenite B2.

Analysis of Other Works on HT-SMAs Inspired by Firstov Studies

Firstov's work in 2015 initiated a promising new class of high-entropy NiTi-like shape memory alloys, (TiHfZr)(NiCoCu). Subsequently, several authors, such as Lee et al. [38], Peltier et al. [24, 37], Thiercelin et al. [31], Yaacoub et al. [28], Chen et al. [27], Rehman et al. [39], Chang et al. [40, 41], Piorunek et al. [29, 42], designed new alloys inspired from Fistov's approach. Figure 2 shows the chemical composition of these alloys and their austenite-to-martensite transformation start temperatures (martensite start or M_s) obtained from differential scanning calorimetry (DSC) measurements. The temperatures ranging from − 34 to 591 °C illustrate a transition zone between superelastic alloys (M_s below 25 °C) and shape memory alloys (M_s above 25 °C) that correspond to a fully austenitic structure or a combination of austenitic and martensitic phases, respectively, as shown in Fig. 1. Nevertheless, by analyzing the M_s temperature given in the different works cited above, it must be pointed out that the M_s have not been measured necessarily in the same metallurgical state of the alloy. In fact, this state depends on the processing procedure, which can vary from one study to another. That explains the noticed differences between some alloys for an identical chemical composition. A criterion of metallurgical state, based on the DSC measurements, is given in the following section. Table 2 presents all the alloys of the $(TiHfZr)_{50}(Ni_XCo_YCu_Z)_{50}$ system listed in the literature. This table shows that certain alloys, such as $(TiHfZr)_{50}Ni_{25}Cu_{25}$ and $(TiHfZr)_{50}Ni_{25}Co_{10}Cu_{15}$ are studied in several works. Table 2 shows that the results of the M_s transformation temperatures of the same alloy vary from one study to another, showing the importance of the metallurgical state of the alloys considered to construct the SMAs databases [31]. In that sense, one can mention the variation of 191 °C between the Firstov study [12] and that carried out by Yaacoub et al. [28] on the $(TiHfZr)_{50}Ni_{25}Co_{10}Cu_{15}$ alloy used for the training of the artificial intelligence-based approach proposed by Thiercelin et al. [31]. It is important to stress that the experimental results of Firstov et al. [12] and Chang et al. [40] are based on the study of HE-SMAs in a metallurgical state after casting or 'as-cast' state. These non-homogenized alloys show wide hysteresis inducing hence a large gap between the temperatures M_s and M_f as shown in Table 2. Indeed, the mean value of $|M_s\text{-}M_f|$ is up to 80 °C for the result presented by Firstov et al. [12] and about 93 °C for those presented by Chang et al. [40].

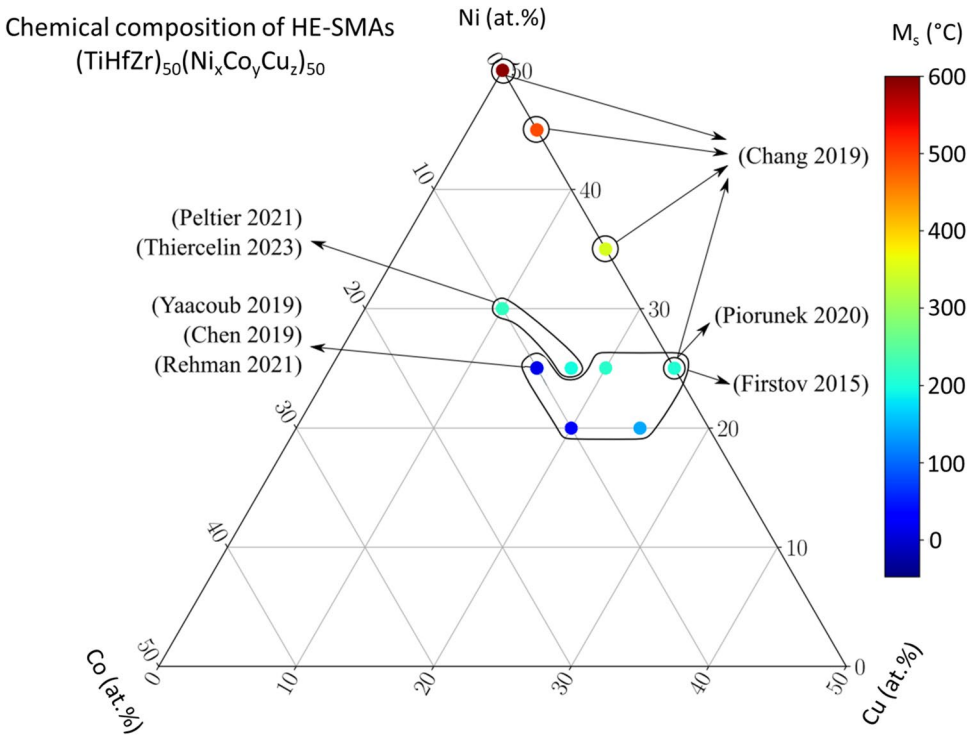

Fig. 2 M_s transformation temperatures of different alloys in studies based on the pseudo-ternary diagram proposed by Firstov. It is worth noticing that the temperatures ranging from − 34 to 591 °C illustrate a transition zone between austenitic state (M_s below 25 °C) and a combination of austenitic and martensitic states (M_s above 25 °C)

Table 2 HE-SMAs of the $(TiHfZr)_{50}NiCoCu$ system and the related M_s temperatures found in the literature

Alloys		Alloying composition (at.%) Ni	Cu	Co	Ti	Hf	Zr	M_s (°C)	$\lvert M_s\text{-}M_f\rvert$ (°C)
Firstov 2015	[12]	25	25	0	16.667	16.667	16.667	227	115
Firstov 2015	[12]	25	20	5	16.667	16.667	16.667	181	49
Firstov 2015	[12]	25	15	10	16.667	16.667	16.667	157	57
Firstov 2015	[12]	20	25	5	16.667	16.667	16.667	103	117
Firstov 2015	[12]	20	20	10	16.667	16.667	16.667	-10	63
Chang 2019	[40-41]	50	0	0	16.667	16.667	16.667	591	79
Chang 2019	[40-41]	45	5	0	16.667	16.667	16.667	482	154
Chang 2019	[40-41]	35	15	0	16.667	16.667	16.667	328	109
Chang 2019	[40-41]	25	25	0	16.667	16.667	16.667	197	32
Chen 2019	[27]	25	15	10	16.667	16.667	16.667	36	120
Lee 2019	[38]	25	15	10	16.667	16.667	16.667	3	51
Yaacoub 2019	[28]	25	15	10	16.667	16.667	16.667	-34	24
Piorunek 2020	[29, 42]	25	25	0	16.667	16.667	16.667	175	38
Rehman 2021	[39]	25	15	10	16.667	16.667	16.667	54	39
Peltier 2021	[37]	25	17.5	7.5	16.667	16.667	16.667	198	32
Peltier 2021	[37]	30	10	10	16.667	16.667	16.667	188	39

Same chemical composition alloys

M_s (°C) 600 500 400 300 200 100 0

$\lvert M_s\text{-}M_f\rvert$ (°C) 180 150 120 90 60 30 0

From Experimental Data to Numerical Predictive Models

Considering the multi-component alloys, CCAs and HEAs, metallurgy should take advantage of "machine learning" concepts to explore the potential combination of the large compositional space of chemical elements. This will lead to optimized alloys to meet the industrial needs in terms of application requirements or to assess other sustainability criteria. For the NiTi-like alloy design, Peltier et al. [37] proposed a linear regression model aimed at predicting martensitic transformation. Nevertheless, this model, called as "Peltier model," has been calibrated considering a small database of only 16 alloys and it has been limited to only some high-entropy alloys. In addition, the linear approach was found to be unsuitable for exploring the full compositional space of multi-component alloys containing more than 4 chemical elements. Thiercelin et al. overcome this limitation [31], by improving the NiTi-like HE-SMAs database proposed by Peltier et al. [43] (https://data.mendeley.com/datasets/z6j6g3b9yf/1; https://doi.org/10.17632/z6j6g3b9yf.1). This database has enriched the one given by Peltier et al. [37] containing alloys of simple and complex chemical compositions: 59% binary and ternary alloys, 28% quaternary alloys, and 13% alloys containing 5 and more elements, such as Cu, Co, Fe, Pd, Pt, Au, Zr, Hf, Nb, and Ta. The main advantage of this database resides in the addition of a metallurgical criterion designed to retain only homogenized alloys. This criterion measures the homogeneity of an alloy by computing the difference between the start and the end of the martensitic transformation. A suitable value has been set to be below 50 °C, i.e., $|M_s - M_f| < 50$ °C. This criterion includes the metallurgical approach to the data, ensuring more robustness of experimental data from different research projects. Indeed, when the gap M_s-M_f does not exceed 50 °C, the alloy exhibits a homogenized metallurgical state. In contrast, as observed in the work of Firstov [12], Piorunek [29], and Chang et al. [40] for as-cast or aged alloys, the DSC curves exhibit a significantly broadened exothermic peak, indicating slower and delayed transformations within the material. As a result, this leads to a large M_s-M_f temperature gap. Considering the $|M_s - M_f| < 50$ °C, a physics-informed machine learning model, called as "Thiercelin model" has been developed to predict the martensitic transformation temperature of NiTi-like shape memory alloys containing several chemical elements [31]. This model is based on Extremely Randomized Tree regression algorithm to predict M_s temperature using a selection of 6 thermodynamic descriptors defined using the chemical composition of the alloying elements and the related physical features, namely: the mixing enthalpy, the valence electron concentration, the atomic radius (averaged with its variation coefficient), and the electronegativity (averaged with its variation coefficient). The model was trained using 80% of the total database. As the amount of binary, ternary, quaternary, and high-entropy alloys is not equal, a proportion of 80% is extracted for each alloy class to be representative of the database. In addition, due to the reduced number of alloys in the database, a K-cross validation method using 100 random splits was used to assure the robustness of the algorithm. It is observed that accuracy decreases as the number of elements increases, with an average error of over 65 °C for the HEA predictions.

Figure 3 shows the extrapolation of this approach on all $(TiHfZr)_{50}(Ni_XCo_YCu_Z)_{50}$ alloy combinations. It is important to mention that the Thiercelin model has been deployed in two ways using different databases as mentioned in the introduction. The first way exploited the "global database," which contains binary, ternary, quaternary, quinary, and senary TiHfZrNiCoCu HE-HT-SMAs including data from papers by Firstov et al. without any metallurgical state

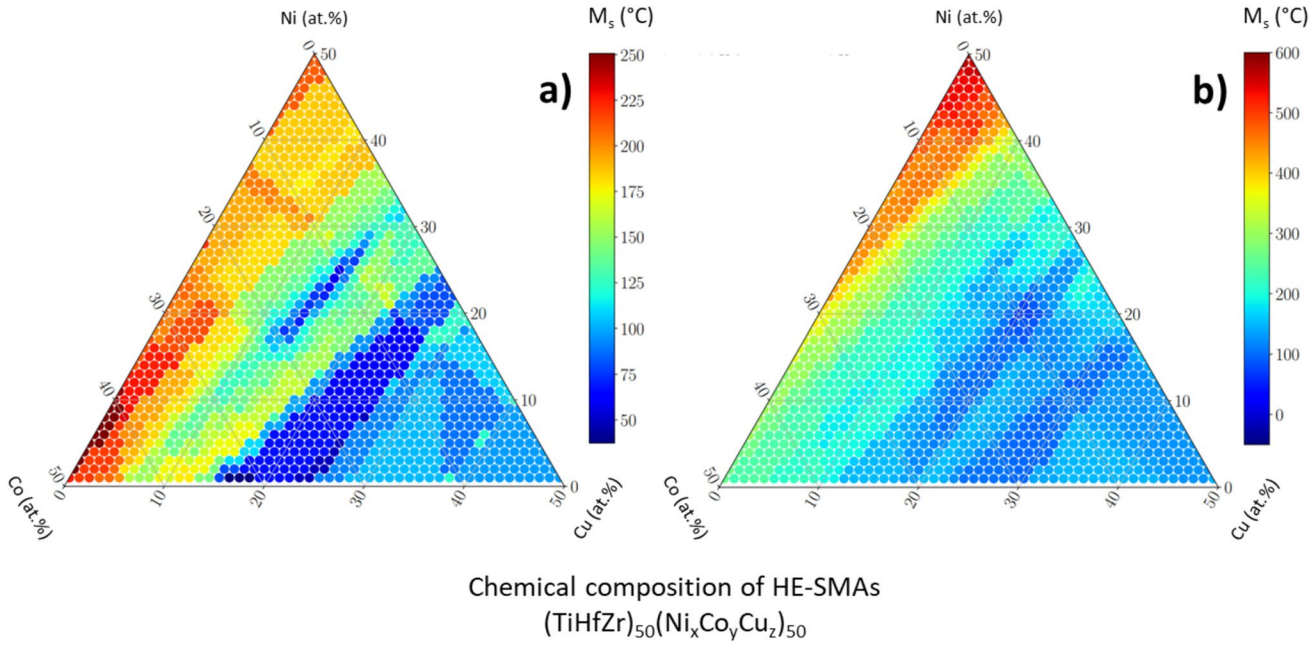

Fig. 3 Graphical representation of the Thiercelin model applied to $(TiHfZr)_{50}(Ni_XCo_YCu_Z)_{50}$ alloys: **a** the results of the model exploiting the "reduced database," **b** the results of the model based on the "global database" regardless the metallurgical state of the alloy

criterion. The second has been limited to the "reduced database" considering only the NiTi-like alloys submitted to homogenization heat treatment for which the difference between M_s and M_f is less than 50 °C. The results limited to the homogenized alloys (reduced database) are illustrated in Fig. 3a, whereas the predictions using the reduced database version are plotted in Fig. 3b. It should be noted that the two representations (Fig. 3a and b) are very distinct. In the reduced version, the results, providing M_s transformation temperatures range from 0 to 300 °C, whereas in the global version, M_s transformation temperatures range from 0 to 600 °C. These differences are due to the use of data from Chang et al. [40], which shows a quaternary $(TiHfZr)_{50}Ni_{50}$ alloy with M_s transformation temperatures of 591 °C considering the metallurgical state criterion, $|M_s\text{-}M_f|$ equal to 79 °C, which is above of the suitable limit value of 50 °C.

In Fig. 1a, Firstov et al. [21–23] demonstrated the existence of 2 zones on the pseudo-ternary diagram: one where the alloys are martensitic with transformation temperatures M_s above 25 °C (presence of the B19' phase at room temperature in Fig. 1b) and the second, larger zone where the alloys are austenitic (presence of the B2 phase at room temperature in Fig. 1c). Conversely to Firstov et al., the Thiercelin model results in Fig. 3a show only one zone since all alloys have M_s transformation temperatures above 50 °C. However, it should be noted that Thiercelin et al. explained that their model has a mean absolute error of 35 °C and 70 °C for 4 quaternary alloys, and HEAs, respectively. Therefore, a M_s prediction below 100 °C implies necessarily that the considered alloys exhibit an unknown metallurgical state, which is in an unhomogenized metallurgical state.

In addition, to further extend the work by Firstov et al. on NiTi-like HE-SMAs, Rehman et al. [39] have studied homogenized non-equimolar NiTi-like compositions, i.e., alloys with the proportion of Ti-like (Ti, Hf, Zr) and Ni-like (Ni, Co, Cu) different from 50 to 50 at.%. Indeed, the authors proposed the study of 4 alloys $(Ti_{1/3}Hf_{1/3}Zr_{1/3})_X(Ni_{1/2}Co_{1/5}Cu_{3/10})_{100\text{-}X}$ where X is replaced by 50, 50.5, 51, and 52 at.% given in Table 3.

In what follows, the numerical predictions are firstly compared to the experimental findings by Rehman et al. [39] considering 4 alloys (TiHfZr)(NiCoCu) where the alloying elements content, given in Table 3, are close to those studied by Firstov et al. In a second time, the M_s temperatures predicted by Thiercelin model are compared to the experimental results provided by Resnina et al. [44–47], Zadeh et al. [36], Chang et al. [48], Kuo et al. [49], and Pang et al. [50] considering more than 30 new chemical compositions of (TiHfZr)(NiCoCu) whose contents are non-equiatomic or totally different from those studied by Firstov et al., as detailed in Table 4.

Comparison of the Numerical Predictions Against Rehman et al. Experimental Results

The experimental results of Rehman et al. [39], previously used as training and validation data [43] for the Thiercelin model, are investigated and compared with the numerical

Table 3 Experimental data from Rehman [39] Vs calculated data [31, 37]

$(Ti_{1/3}Hf_{1/3}Zr_{1/3})_X(Ni_{1/2}Co_{1/5}Cu_{3/10})_{100-X}$		M_s temperature (°C)			
		Experimental	Calculated		
X	Alloying compositions (at. %)	Rehman et al.	Peltier et al.	Thiercelin et al. Global Database	Thiercelin et al. Reduced Database
50.0	$Ti_{16.7}Hf_{16.7}Zr_{16.7}Ni_{25.0}Co_{10.0}Cu_{15.0}$	54	153 99	58 4	93 39
50.5	$Ti_{16.8}Hf_{16.8}Zr_{16.8}Ni_{24.7}Co_{9.8}Cu_{14.8}$	168	170 2	149 19	152 16
51.0	$Ti_{17.0}Hf_{17.0}Zr_{17.0}Ni_{24.5}Co_{9.7}Cu_{14.7}$	170	185 15	150 20	159 11
52.0	$Ti_{17.3}Hf_{17.3}Zr_{17.3}Ni_{24.0}Co_{9.3}Cu_{14.3}$	183	220 37	203 20	183 0
Mean value for each model →			39	16	17
Difference between model and experimental					

results of two prediction approaches, the linear approximation-based model of Peltier et al. [37] as well as the Thiercelin model [31].

The results are summarized and compared in Table 3. The latter shows that both the "global" and "reduced" versions of the results are the predictions using the Thiercelin model [31]. In fact for HE-SMAs, the predicted temperatures show a maximum absolute error of 39 °C with respect to the experimental values. One can remind that the maximum absolute error predicted using the linear approach proposed by Peltier et al. [37] reaches an error level of 99 °C for $(TiHfZr)_{50}(Ni_XCo_YCu_Z)_{50}$ HE-SMAs. However, it can be noticed that the linear model is still accurate as the data-driven model prediction (in both versions) for $X = 50.5$, $X = 51$, and $X = 52$ at.%. This can be explained by the fact that the Peltier model has been based on a specific database of alloys containing only (TiHfZr)(NiCoCu) HE-SMAs with chemical compositions close to those elaborated by Firstov et al., whereas the Thiercelin model is interested in database including low, medium, and high-entropy SMAs.

Figure 4 shows the chemical composition map of NiTi-like alloys given by the Thiercelin model using the reduced database with different values of Ti-like content (X), namely: $X = 50$, 50.5, 51, and 52 at.%. In this figure, the alloy compositions of Rehman et al. [39] are highlighted by red crosses surrounded by black circles. Table 3 and Fig. 4 demonstrate that increasing the Ti-like content increases the M_s transformation temperature regardless the proportion of Ni, Cu, and Co elements.

Comparison of the Numerical Predictions Considering Other Compositions

The numerical predictions are now compared with experimental studies recently published by Resnina et al. [44–47], Zadeh et al. [36], Chang et al. [48], Kuo et al. [49], Pang et al. [50], and Li et al. [51] which provide more than 30 new chemical compositions whose contents are non-equiatomic or completely different from those studied by Firstov et al. as detailed in Table 4. It should be pointed out that the compositions proposed by Resnina et al. [44–47], Li et al. [51], and Zadeh et al. [36] do not allow the use of the linear model proposed by Peltier et al. [37]. In fact, these chemical compositions exceed the validity range of the model (in shaded boxes in Table 4). In fact, unlike the alloy compositions of Rehman et al. in Fig. 3 and Table 3, these new alloys cannot be represented on a pseudo-ternary diagram because their composition of Ti-like elements is not equiatomic. The list of these new alloys includes very specific chemical compositions (at.%), such as $Ti_9Hf_{39}Zr_4Ni_{30}Co_9Cu_9$, $Ti_6Hf_{38}Zr_8Ni_{17}Co_{16}Cu_{15}$, $Ti_9Hf_{32}Zr_{11}Ni_{16}Co_{14}Cu_{18}$ [44–47], in which the element Hafnium predominates, in order to increase the transformation temperatures. It is worth noticing that compared to using the data in Table 3, the average error between the experimental results and the predictions of the two models is higher when using the experimental results in Table 4: 2.6 times higher for the Peltier model and 3.6 times higher for the Thiercelin model. This wide scatter of the calculated results can be explained by the fact that the experimental data of Resnina et al. and, Zadeh et al. are data obtained on alloys in their "as-cast" state without homogenization heat treatment.

Concluding Remarks

This paper provides an overview of the design strategy for (TiHfZr)(NiCoCu) HE-HT-SMAs, starting with the experimental work presented by Firstov at the ESOMAT 2018 international conference in Metz. At the conference, he introduced eight quinary and senary alloys in a pseudo-ternary diagram, $(TiHfZr)_{50}(Ni_XCo_YCu_Z)_{50}$, which exhibited

Table 4 Experimental data from the recent literature Vs calculated data [31, 37]

$(TiHfZr)_X(NiCoCu)_{100-X}$			M_s temperature (°C)			
			Experimental	Calculated		
				Peltier et al. [37]	Thiercelin et al. [31]	
X	Alloying compositions (at.%)				Global Database	Reduced Database
52.0	$Ti_9Hf_{39}Zr_4Ni_{30}Co_9Cu_9$	Resnina et al. [44-47]	419		308 111	418 1
50.0	$Ti_{24}Hf_{26}Ni_{41}Cu_9$	Zadeh et al. [36]	300		167 133	130 170
50.3	$Ti_{25.3}Hf_{25}Ni_{42.7}Cu_7$	Zadeh et al. [36]	299		195 104	150 149
51.5	$Ti_{31.5}Hf_{15}Zr_5Ni_{48.5}$	Pang et al. [50]	291		274 17	277 14
50.0	$Ti_{23.9}Hf_{26}Ni_{41.3}Cu_7$	Zadeh et al. [36]	286		217 69	132 154
51.5	$Ti_{31.5}Hf_{15}Zr_5Ni_{43.5}Cu_5$	Pang et al. [50]	221		139 82	204 17
50.0	$Ti_{20}Hf_{15}Zr_{15}Ni_{35}Cu_{15}$	Kuo et al. [49]	206	150 56	180 26	187 19
50.0	$Ti_{23.1}Hf_{27}Ni_{41.9}Cu_8$	Zadeh et al. [36]	192		226 34	182 10
52.0	$Ti_{17.3}Hf_{17.3}Zr_{17.3}Ni_{24.0}Co_{14.4}Cu_{9.6}$	Rehman et al. [39]	183	212 29	183 0	203 20
52.0	$Ti_6Hf_{38}Zr_8Ni_{17}Co_{16}Cu_{15}$	Resnina et al. [44-47]	172		285 113	426 254
52.0	$Ti_9Hf_{32}Zr_{11}Ni_{16}Co_{14}Cu_{18}$	Resnina et al. [44-47]	172	450 278	258 86	298 126
51.0	$Ti_{17.0}Hf_{17.0}Zr_{17.0}Ni_{24.5}Co_{14.7}Cu_{9.8}$	Rehman et al. [39]	170	180 10	159 11	150 20
50.5	$Ti_{16.8}Hf_{16.8}Zr_{16.8}Ni_{24.7}Co_{14.8}Cu_{9.9}$	Rehman et al. [39]	168	166 2	152 16	126 42
51.5	$Ti_{31.5}Hf_{15}Zr_5Ni_{38.5}Cu_{10}$	Pang et al. [50]	161		99 62	136 25
50.0	$Ti_{20}Hf_{15}Zr_{15}Ni_{35}Cu_{15}$	Chang et al. [48]	160	150 10	180 20	187 27
50.0	$Ti_{25}Hf_{12.5}Zr_{12.5}Ni_{35}Cu_{15}$	Kuo et al. [49]	111	-6 117	101 10	111 0
51.5	$Ti_{31.5}Hf_{15}Zr_5Ni_{33.5}Cu_{15}$	Pang et al. [50]	72	-81 153	24 48	90 18
49.5	$Ti_{22.6}Hf_{27}Ni_{35.4}Cu_{15}$	Zadeh et al. [36]	71		170 99	108 37
51.0	$Ti_{49}Hf_1Zr_1Ni_{47}Co_1Cu_1$	Resnina et al. [44-47]	56		44 12	32 24
50.0	$Ti_{16.7}Hf_{16.7}Zr_{16.7}Ni_{25.0}Co_{15.0}Cu_{10.0}$	Rehman et al. [39]	54	145 91	104 50	58 4
50.5	$Ti_{32.5}Hf_{18}Ni_{32.5}Cu_{17}$	Zadeh et al. [36]	43		-2 45	79 36
50.5	$Ti_{38.4}Hf_{12}Ni_{34.6}Cu_{15}$	Zadeh et al. [36]	39		42 3	58 19
52.0	$Ti_{14}Hf_{23}Zr_{15}Ni_{18}Co_{15}Cu_{15}$	Resnina et al. [44-47]	35	292 257	314 279	291 256
50.0	$Ti_{48}Hf_1Zr_1Ni_{48}Co_1Cu_1$	Resnina et al. [44-47]	34		44 10	27 7
50.0	$Ti_{25}Hf_{25}Ni_{25}Cu_{25}$	Li et al. [51]	27		49 22	42 15
50.5	$Ti_{36.5}Hf_{14}Ni_{32.5}Cu_{17}$	Zadeh et al. [36]	13		5 8	3 10
49.0	$Ti_{47}Hf_1Zr_1Ni_{49}Co_1Cu_1$	Resnina et al. [44-47]	-1		21 22	22 23
51.5	$Ti_{31.5}Hf_{15}Zr_5Ni_{28.5}Cu_{20}$	Pang et al. [50]	-2	-130 128	-3 1	30 32
50.0	$Ti_{40}Hf_5Zr_5Ni_{40}Co_5Cu_5$	Resnina et al. [44-47]	-42		-31 11	35 77
51.0	$Ti_{41}Hf_5Zr_5Ni_{39}Co_5Cu_5$	Resnina et al. [44-47]	-46		-42 4	47 93
49.0	$Ti_{39}Hf_5Zr_5Ni_{41}Co_5Cu_5$	Resnina et al. [44-47]	-99		-28 71	33 132
		Mean value for each model		103	51	59
		Difference between model and experimental				

Chemical compositions close to Firstov

Chemical compositions that exceed the validity range of the Peltier model

It should be pointed out that the alloys developed by Resnina et al. [44–47], Zadeh et al. [36], Chang et al. [48], Kuo et al. [49], Pang et al. [50] and Li et al. [51] have non-equiatomic contents or completely different from those studied by Firstov et al. nor those proposed by Rehman et al. [39]

remarkable properties, particularly in terms of the M_s temperature. The database for (TiHfZr)(NiCoCu) system has since been expanded and enriched through additional research studies, incorporating variations in chemical composition and homogenization heat treatments. Since 2021, numerical models predicting M_s temperature have emerged, paving the way for a data-driven strategy for $(TiHfZr)_{50}(Ni_XCo_YCu_Z)_{50}$ alloys. One such model, proposed by Thiercelin et al., utilizes a database of NiTi-like alloys and physical material descriptors to predict the M_s temperature. In this paper, two predictive models have been applied to the investigated (TiHfZr)(NiCoCu) family which have led to the following concluding remarks:

(1) The Thiercelin model exploits the experimental data of numerous researchers through a detailed database on the metallurgical system of (TiHfZr)(NiCoCu) shape memory alloys. The Thiercelin model is suitable for the design of HE-HT-SMAs with complex (TiHfZr)(NiCoCu) type compositions. This model represents a breakthrough in HE-SMA design since it is now pos-

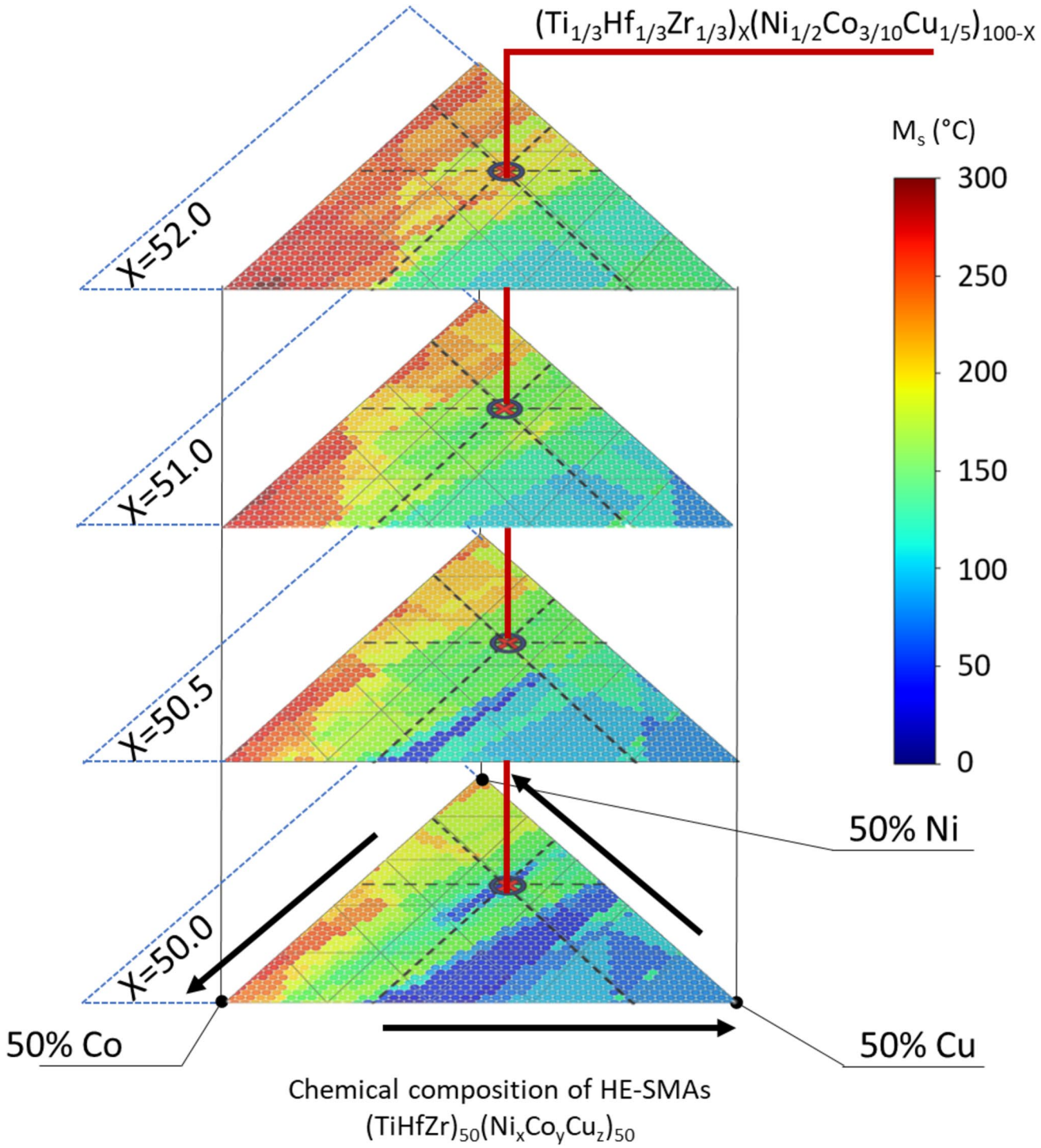

Fig. 4 Graphical representation of the M_s transformation temperatures given by the Thiercelin model (using the reduced database) applied to $(TiHfZr)_X(Ni_xCo_yCu_z)_{100-X}$ alloys. The representation shows the model response for 4 values of X: $X=50$, $X=50.5$, $X=51$, and $X=52$. The blue circles show the 4 alloys designed by Rehman et al. [39]

sible to consistently optimize alloys without having to produce a large number of alloys experimentally.

(2) The results from the Thiercelin model are far from the experimental results proposed by Firstov in 2015, Resnina and Zadeh in 2024. This difference is explained by the fact that these authors used as-cast alloys without homogenization treatment.

(3) The results given by the Thiercelin model on (TiHfZr)(NiCoCu) alloys are very close to the experimental results of Rehman et al., Pang et al., Kuo et al., and Chang et al. who use alloys in their homogenized state.
(4) The database used in this work has been built in such a way that it can be easily enriched by input from other researchers (collaborative works). These further developments and data inputs will be beneficial for the HEAs community to expand the compositional space studied in the (TiHfZr)(NiCoCu) alloys. It will be carried out by exploring further alloys whose contents of Hf, Co, Zr, and Cu exceed those of the current (TiHfZr)(NiCoCu) alloys. This will enrich the training and testing stages of the Thiercelin model.

The design strategy for the (TiHfZr)(NiCoCu) HE-HT-SMA family is increasingly being generalized to the development of Multi-Principal Element Alloys (MPEAs). The developed approaches should combine numerical methods and experimental data to create data-driven tools that can accelerate alloy design optimization. Additionally, the critical need for sourcing materials sustainably must be integrated into alloy design strategies, potentially guided by computational approaches. While metallurgy has long been a phenomenological and experimental science, it now requires efficiency and acceleration through artificial intelligence, as reported in a review paper by Dewangan et al. [52].

Supplementary data

Supplementary data related to this article can be found at: https://data.mendeley.com/datasets/z6j6g3b9yf/1; https://doi.org/10.17632/z6j6g3b9yf.1 [43]. The authors offer their help in using the model, encouraging readers to produce their HE-SMAs.

Acknowledgements This research sounds like a tribute to the work of Firstov et al.. It was supported by the M^{2}ARTS research group of the LEM3 laboratory. The authors thank the facilities of the LEM3 laboratory ("Procédés", "MicroMat", and "MécaRhéo") and the "Cassiopée" intensive computing platform at the Ecole Nationale Supérieure d'Arts et Métiers. The authors would like to thank our KIT colleagues Eva Guilbert and Nicolas Ruchty for their help, which greatly facilitated this study. The authors will enrich the database proposed by Thiercelin et al. [43] by appending the recent state of the art on the new HE-SMAs compositions presented in the paper. The updated database will be achieved to improve the existing Thiercelin model to make it more efficient and predictive for the benefits of the scientific community. Although this article deals in part with artificial intelligence, the authors vouch for the authenticity of its contents. Artificial intelligence was used in the context of metallurgy and alloy design and in no way in the writing of this article.

Funding Open access funding provided by Arts et Metiers Institute of Technology.

Declarations

Conflict of interest The authors have no conflicts to disclose.

References

1. Buehler W, Wang F (1968) A summary of recent research on the nitinol alloys and their potential application in ocean engineering. Ocean Eng 1:105–120. https://doi.org/10.1016/0029-8018(68)90019-X
2. Mohd Jani J, Leary M, Subic A, Gibson MA (2014) A review of shape memory alloy research, applications and opportunities. Mater Des 56:1078–1113. https://doi.org/10.1016/j.matdes.2013.11.084
3. Frenzel J, George EP, Dlouhy A et al (2010) Influence of Ni on martensitic phase transformations in NiTi shape memory alloys. Acta Mater 58:3444–3458. https://doi.org/10.1016/j.actamat.2010.02.019
4. Frenzel J, Wieczorek A, Opahle I et al (2015) On the effect of alloy composition on martensite start temperatures and latent heats in Ni – Ti-based shape memory alloys. Acta Mater 90:213–231. https://doi.org/10.1016/j.actamat.2015.02.029
5. Ma J, Karaman I, Noebe RD (2010) High temperature shape memory alloys. Int Mater Rev 55:257–315. https://doi.org/10.1179/095066010x12646898728363
6. Karakoc O, Hayrettin C, Canadinc D, Karaman I (2018) Role of applied stress level on the actuation fatigue behavior of NiTiHf high temperature shape memory alloys. Acta Mater 153:156–168. https://doi.org/10.1016/j.actamat.2018.04.021
7. Karakoc O, Hayrettin C, Bass M et al (2017) Effects of upper cycle temperature on the actuation fatigue response of NiTiHf high temperature shape memory alloys. Acta Mater 138:185–197. https://doi.org/10.1016/j.actamat.2017.07.035
8. Bigelow GS, Padula SA, Garg A et al (2010) Characterization of ternary NiTiPd high-temperature shape-memory alloys under load-biased thermal cycling. Metall Mater Trans A 41:3065–3079. https://doi.org/10.1007/s11661-010-0365-5
9. Achard FK (1788) Recherches sur les propriétés des alliages métalliques. https://books.google.fr/books?id=3649nQEACAAJ
10. Cantor B, Chang ITH, Knight P, Vincent AJB (2004) Microstructural development in equiatomic multicomponent alloys. Mater Sci Eng A 375–377:213–218. https://doi.org/10.1016/j.msea.2003.10.257
11. Cantor B (2020) Multicomponent high-entropy Cantor alloys. Progress Mater Sci. https://doi.org/10.1016/j.pmatsci.2020.100754

12. Firstov GS, Kosorukova TA, Koval YN, Odnosum VV (2015) High entropy shape memory alloys. Mater Today: Proc 2:S499–S503. https://doi.org/10.1016/j.matpr.2015.07.335
13. Casalena L, Bigelow GS, Gao Y et al (2017) Mechanical behavior and microstructural analysis of NiTi-40Au shape memory alloys exhibiting work output above 400 °C. Intermetallics 86:33–44. https://doi.org/10.1016/j.intermet.2017.03.005
14. Ramaiah KV, Saikrishna CN, Sujata M et al (2019) NiTiPt shape memory alloy: microstructure and transformation behaviour. ISSS J Micro Smart Syst 8:81–88. https://doi.org/10.1007/s41683-019-00039-9
15. Lin B, Gall K, Maier HJ, Waldron R (2009) Structure and thermomechanical behavior of NiTiPt shape memory alloy wires. Acta Biomater 5:257–267. https://doi.org/10.1016/j.actbio.2008.07.015
16. Monroe JA, Karaman I, Lagoudas DC et al (2011) Determining recoverable and irrecoverable contributions to accumulated strain in a NiTiPd high-temperature shape memory alloy during thermomechanical cycling. Scr Mater 65:123–126. https://doi.org/10.1016/j.scriptamat.2011.03.019
17. Khaleghi F, Tajally M, Emadoddin E, Mohri M (2019) The investigation of the mechanical properties of graded high-temperature shape memory Ti-Ni-Pd alloy. J Alloys Compd 787:882–892. https://doi.org/10.1016/j.jallcom.2019.02.142
18. Motemani Y, Buenconsejo PJS, Ludwig A (2015) Recent developments in high-temperature shape memory thin films. Shape Mem Superelast 1:450–459. https://doi.org/10.1007/s40830-015-0041-0
19. Buenconsejo PJS, Ludwig A (2014) Composition–structure–function diagrams of Ti–Ni–Au thin film shape memory alloys. ACS Comb Sci 16:678–685. https://doi.org/10.1021/co5000745
20. Canadinc D, Trehern W, Ma J et al (2019) Ultra-high temperature multi-component shape memory alloys. Scr Mater 158:83–87. https://doi.org/10.1016/j.scriptamat.2018.08.019
21. Firstova G, Timoshevski A, Kosorukova T et al (2015) Electronic and crystal structure of the high entropy TiZrHfCoNiCu intermetallics undergoing martensitic transformation. MATEC Web Conf. https://doi.org/10.1051/matecconf/20153306006
22. Firstov GS (2018) Functional metallic shape memory materials: state of the art and application prospects. Visnik Nacional'noi' academii' nauk Ukrai'ni 06:19–34. https://doi.org/10.15407/visn2018.06.019
23. Firstov GS (2023) Development of high-entropy shape-memory alloys: structure and properties. Prog Phys Met. https://doi.org/10.15407/ufm.24.04.819
24. Peltier L, Lohmuller P, Meraghni F et al (2020) Investigation and composition characterization of a "NiTi-like" alloy combining high temperature shape memory and high entropy. Shape Mem Superelast. https://doi.org/10.1007/s40830-020-00290-2
25. Peltier L, Berveiller S, Meraghni F et al (2021) Martensite transformation and superelasticity at high temperature of $(TiHfZr)_{74}(NbTa)_{26}$ high-entropy shape memory alloy. Shape Mem Superelast. https://doi.org/10.1007/s40830-021-00323-4
26. Peltier L, Lohmuller P, Meraghni F et al (2022) Damping behavior in a wide temperature range of FeMn-like high entropy shape memory alloys. Shape Mem Superelast. https://doi.org/10.1007/s40830-022-00381-2
27. Chen CH, Chen YJ (2019) Shape memory characteristics of $(TiZrHf)_{50}Ni_{25}Co_{10}Cu_{15}$ high entropy shape memory alloy. Scr Mater 162:185–189. https://doi.org/10.1016/j.scriptamat.2018.11.023
28. Yaacoub J, Abuzaid W, Brenne F, Sehitoglu H (2020) Superelasticity of $(TiZrHf)_{50}Ni_{25}Co_{10}Cu_{15}$ high entropy shape memory alloy. Scr Mater 186:43–47. https://doi.org/10.1016/j.scriptamat.2020.04.017
29. Piorunek D, Frenzel J, Niels J et al (2020) Intermetallics chemical complexity, microstructure and martensitic transformation in high entropy shape memory alloys. Intermetallics. https://doi.org/10.1016/j.intermet.2020.106792
30. Hart GLW, Mueller T, Toher C, Curtarolo S (2021) Machine learning for alloys. Nat Rev Mater 6:730–755. https://doi.org/10.1038/s41578-021-00340-w
31. Thiercelin L, Peltier L, Meraghni F (2024) Physics-informed machine learning prediction of the martensitic transformation temperature for the design of "NiTi-like" high entropy shape memory alloys. Comput Mater Sci. https://doi.org/10.1016/j.commatsci.2023.112578
32. Liu S, Kappes BB, Amin-ahmadi B et al (2021) Physics-informed machine learning for composition—process—property design: shape memory alloy demonstration. Appl Mater Today 22:100898. https://doi.org/10.1016/j.apmt.2020.100898
33. He S, Wang Y, Zhang Z et al (2023) Interpretable machine learning workflow for evaluation of the transformation temperatures of TiZrHfNiCoCu high entropy shape memory alloys. Mater Des 225:111513. https://doi.org/10.1016/j.matdes.2022.111513
34. Kankanamge UMHU, Reiner J, Ma X et al (2022) Machine learning guided alloy design of high-temperature NiTiHf shape memory alloys. J Mater Sci 57:19447–19465. https://doi.org/10.1007/s10853-022-07793-6
35. Saedi S, Raji H (2024) Next-generation multicomponent SMAs: leveraging HEA empirical parameters. Scr Mater 252:116262. https://doi.org/10.1016/j.scriptamat.2024.116262
36. Hossein Zadeh S, Cakirhan C, Khatamsaz D et al (2024) Data-driven study of composition-dependent phase compatibility in NiTi shape memory alloys. Mater Des 244:113096. https://doi.org/10.1016/j.matdes.2024.113096
37. Peltier L, Meraghni F, Berveiller S et al (2021) Relationship between chemical composition and Ms temperature in high-entropy shape memory alloys. Shape Mem Superelast 7:438–446. https://doi.org/10.1007/s40830-021-00342-1
38. Lee HC, Chen YJ, Chen CH (2019) Effect of solution treatment on the shape memory functions of $(TiZrHf)_{50}Ni_{25}Co_{10}Cu_{15}$ high entropy shape memory alloy. Entropy 21:1027
39. Rehman IU, Li S, Nam TH (2021) Transformation materials behavior and superelasticity of TiZrHfNiCoCu multi-component high-temperature shape memory alloys. J Alloys Compd. https://doi.org/10.1016/j.jallcom.2021.161108
40. Chang S, Lin P, Tsai C (2019) High-temperature martensitic transformation of CuNiHfTiZr high- entropy alloys. Sci Rep. https://doi.org/10.1038/s41598-019-55762-y
41. Chang S-H, Kao W-P, Hsiao K-Y et al (2021) High-temperature shape memory properties of $Cu_{15}Ni_{35}Ti_{25}Hf_{12.5}Zr_{12.5}$ high-entropy alloy. J Mater Res Technol 14:1235–1242. https://doi.org/10.1016/j.jmrt.2021.07.008
42. Piorunek D, Oluwabi O, Frenzel J et al (2020) Effect of off-stoichiometric compositions on microstructures and phase transformation behavior in Ni-Cu-Pd-Ti-Zr-Hf high entropy shape memory alloys. J Alloys Compd. https://doi.org/10.1016/j.jallcom.2020.157467
43. Thiercelin L, Peltier L, Meraghni F (2023) Database providing Ms temperature for NiTi-like alloys. UPDATE_Oct.2023, Mendeley Data, V1. https://doi.org/10.17632/z6j6g3b9yf.1
44. Resnina N, Belyaev S, Ponikarova I et al (2024) Ultra-high temperature Ti-Hf-Zr-Ni-Cu-Co shape memory alloy. Mater Lett 370:136847. https://doi.org/10.1016/j.matlet.2024.136847
45. Resnina N, Belyaev S, Bazlov A et al (2023) The influence of the doping elements on the structure and the martensitic transformations in the $Ti_{50-2x}Hf_xZr_xNi_{50-2x}Cu_xCo_x$ shape memory alloys. Mater Lett 333:133670. https://doi.org/10.1016/j.matlet.2022.133670
46. Resnina N, Belyaev S, Sibirev A et al (2023) The influence of the chemical composition of the Ti-Hf-Zr-Ni-Cu-Co shape memory alloys on the structure and the martensitic transformations. J Alloys Compd 968:172040. https://doi.org/10.1016/j.jallcom.2023.172040

47. Resnina N, Belyaev S, Bazlov A et al (2024) Palladium-free multicomponent high temperature shape memory alloys. Int J Eng Sci 197:104027. https://doi.org/10.1016/j.ijengsci.2024.104027
48. Chang Y-T, Lee M-H, Chu M-W, Chen C-H (2022) Phase formations and microstructures of $Ti_{20}Zr_{15}Hf_{15}Ni_{35}Cu_{15}$ high-entropy shape memory alloy under different aging conditions. Mater Today Adv 14:100223. https://doi.org/10.1016/j.mtadv.2022.100223
49. Kuo S-Y, Kao W-P, Chang S-H et al (2023) Effect of homogenization on the transformation temperatures and mechanical properties of $Cu_{15}Ni_{35}Hf_{12.5}Ti_{25}Zr_{12.5}$ and $Cu_{15}Ni_{35}Hf_{15}Ti_{20}Zr_{15}$ high-entropy shape memory alloys. Materials 16:3212. https://doi.org/10.3390/ma16083212
50. Pang J, Dang P, Tian J et al (2024) Effect of Cu content on martensitic transformation and shape memory behavior in $Ti_{31.5}Hf_{15}Zr_5Ni_{48.5-x}Cu_x$ alloys. J Mater Sci 59:11096–11109. https://doi.org/10.1007/s10853-024-09820-0
51. Li QZ, Wang HY, Shuitcev AV et al (2024) Microstructure and martensitic transformation in $Ni_{25}Ti_{25}Hf_{25}Cu_{25}$ medium entropy shape memory alloy. Intermetallics 168:108254. https://doi.org/10.1016/j.intermet.2024.108254
52. Dewangan SK, Nagarjuna C, Jain R et al (2023) Review on applications of artificial neural networks to develop high entropy alloys: a state-of-the-art technique. Mater Today Commun. https://doi.org/10.1016/j.mtcomm.2023.107298